A Polymer/TiO_2- Nanorod Nanocomposite Optical Memristor Device

A. H. Jaafar†,[a, b] M. M. Al Chawa†,[c] F. Cheng,[d] S.M. Kelly,[d] R. Picos,[e] R. Tetzlaff[c] and N. T. Kemp[a, f,] *

[a] Department of Physics and Mathematics, University of Hull, Cottingham Rd, Hull, HU6 7RX, United Kingdom

[b] School of Electronics and Computer Science, University of Southampton, Southampton, SO17 1BJ, United Kingdom

[c] Faculty of Electrical and Computer Engineering, Institute of Circuits and Systems, Technische Universität Dresden, 01069 Dresden, Germany,

[d] Department of Chemistry and Biochemistry, University of Hull, Cottingham Rd, Hull, HU6 7RX, United Kingdom

[e] Industrial Engineering and Construction Department, Universitat de les Illes, Balears, 07122 Palma, Spain

[f] School of Physics and Astronomy, University of Nottingham, Nottingham, NG7 2RD, UK

† These authors contributed equally to this work.

* Author to whom correspondence should be addressed. Electronic mail: N.Kemp@hull.ac.uk

Keywords: optical memristor, nanorod, titanium dioxide, PDR1A, resistive switching, RRAM, resistive memory, charge-flux model

Abstract

Modulation of resistive switching memory by light opens the route to new optoelectronic devices that can be controlled both optically and electronically. Applications include integrated circuits with memory elements switchable by light and neuromorphic computing with optically reconfigurable and tunable synaptic circuits. We report on a unique nanocomposite resistive switching material and device made from a low concentration (~0.1% by mass) of titanium dioxide nanorods (TiO_2-NRs) embedded within the azobenzene polymer, *poly*(disperse red 1 acrylate, PDR1A). The device exhibits both reversible electronic memristor switching and reversible polarization dependent optical switching. Optical irradiation by circularly polarized light causes a *trans-cis* photochemical isomerization that modifies the conformation and orientation of the photoactive azo-unit within the polymer. The resulting expansion of the composite (PDR1A/ TiO_2-NR) polymer film modifies the conduction pathway, facilitated by the presence of the TiO_2-NRs, as a semiconductor material, through the (PDR1A/ TiO_2-NR) polymer film, which provides a sensitive means to control resistive switching in the device. The effect is reversible by changing the polarization state of the incident light. A charge-flux memristor model successfully reproduces the current-voltage hysteresis loops and threshold switching properties of the device, as well as the effect of the illumination on the electrical characteristics.

I. Introduction

The modulation of resistive memory devices by light has numerous applications including light-switchable memory elements in optical communications[1] and photonic integrated circuits,[2] fast in-memory computer vision systems,[3,4] and light tunable artificial synapses in neuromorphic computing.[5,6,7] Recently we have pioneered several optical memristor types based on polymers mixed with metal nanoparticles,[8] ZnO nanorods,[9] and graphene oxide.[10] The use of hybrid materials in memristor devices is generally much less studied than their solid-state counterparts. However, blending organic (polymer) and inorganic (metals, oxides) components, offer a number of advantages, including low cost, easy solution-based processing[11] via screen-printing or spin-coating, and easy tailoring of the materials mechanical, electronic and optical properties through chemical synthesis.[12–19] In recent years hybrid materials have shown significant improvements in their performance for memory applications. Some of the highlights include, very fast switching speeds (less than 25 ns),[20] large OFF/ON resistance ratios (up to 10^5 orders of magnitude),[21] high endurance (more than 10^5 cycles) combined with long data storage retention (more than 10^6 s),[22] and high storage density integration.[23–25]

In this article, we report on a new optical memristor device based on a hybrid material of TiO_2 nanorods embedded within an optically active polymer. TiO_2 is the classic memristor material, first used by Stanley Williams at HP Labs[26] to show the link between resistive switching in thin metal oxide films and Leon Chua's theoretical description of memristors.[27] Whilst much research has focused on improving the materials and device switching properties of TiO_2 devices, there are few reports of TiO_2 nanorods used in memristor device. Very recently hydrothermally grown free-standing TiO_2 nanorod arrays have been used to make memristor devices[28,29] but to the best of our knowledge there are no reports on the fabrication of a hybrid polymer/TiO_2 NR devices and no study on optical switching effects in TiO_2 devices.

Hybrid materials consisting of metal oxide nanorods embedded within a polymer provide an extremely simple and low cost route to making non-volatile memristor devices[30]. Advantages include the fabrication under ambient conditions (room temperature, vacuum-free) using simple solution processing techniques (spin-coating[18], inkjet and screen-printing technologies and electrochemical methods[17]) and large-area coverage on inexpensive and lightweight substrates. Fine-tuning of the switching properties can be obtained by changing the nanorod concentration[8] and device functionality can be introduced via the polymer, e.g. light controllable synaptic learning[9]. In particular, the high aspect ratio of the nanorods can be used to create conducting pathways within the material to minimize the volume fraction of the nanorod material, as shown in this study.

To impart optical functionality to the devices we have used the azobenzene polymer, poly(disperse red 1 acrylate), referred to now as PDR1A. PDR1A is an optically active polymer that undergoes a reversible *trans-cis* photochemical isomerization upon optical excitation,[31,32] as shown in Fig. 1c). Associated with this is a significant photomechanical response,[33] caused by the progressive alignment of chromophores from repeated *trans-cis-trans* cycling, which occurs because of the overlap of the two absorption bands for the *trans-cis* and *cis-trans* transitions.[34,35,36,37] Circularly polarized light aligns the chromophores in the direction of the beam, causing the thickness of the film to increase whereas linearly polarized light causes a reduction in the thickness of a thin-film when the beam is directed perpendicular to the surface, as reported previously.[8,9]

II. Device Fabrication and Experimental Methods

The test memristor devices consist of a uniform thin (200 nm) nanocomposite layer consisting of surface-stabilized titanium dioxide nanorods (TiO_2 NRs) [38–40] uniformly dispersed within a commercially-available (Sigma Aldrich) and optically-active azobenzene polymer, i.e., Poly(Disperse Red 1 Acrylate (PDR1A) sandwiched between a bottom ITO electrode and a top aluminum electrode, as shown in Fig. 1a). The length and diameter of the titanium dioxide nanorods (TiO_2-NRs) are approximately 20 nm and 3 nm, respectively, as shown by the TEM image shown in Fig. 1b), giving an aspect ratio of between 5 and 8, respectively. The synthesis, purification and characterization of the surface-stabilized titanium dioxide nanorods (TiO_2 NRs) has been reported previously.[38–40] The nanocomposite polymer film (PDR1A/TiO_2-NRs) was deposited on the substrate surface from solution using a standard spin-coating process (1000 rpm for 30 s). The solution of PDR1A and TiO_2 NRs, used in the spin-coating process, was prepared by mixing a solution of PDR1A in tetrahydrofuran (5% weight/weight) with a solution of the TiO_2-NRs in chloroform (1% weight/weight). The volume of the TiO_2-NRs solution was varied to yield composite PDR1A/TiO_2-NR polymer films with a different mass ratio (Rm) of the TiO_2-NRs, i.e., 0.01 wt%, 0.05 wt% and 0.1 wt%, in the PDR1A. After deposition by spin-coating, the PDR1A/TiO_2-NR layer was annealed at ~90°C for 20 minutes in air in order to dry the film and remove residual solvent. The top conducting aluminum metal electrode with a uniform thickness (200 nm) was deposited on top of the solid PDR1A/TiO_2-NR polymer layer as a series of 400 μm diameter circles by a thermal evaporation process. The I-V sweeps were carried out using a probe station equipped with an HP4140B source-meter unit. Photomechanical expansion/contraction of the PDR1A/TiO_2-NR layer was induced by irradiation with either circular or linearly polarized light generated from an Argon ion laser tuned to 514 nm. The spot size of the laser beam had a diameter of 3 mm and the average power per unit area for the exposed device was 180 mW cm^{-2}.

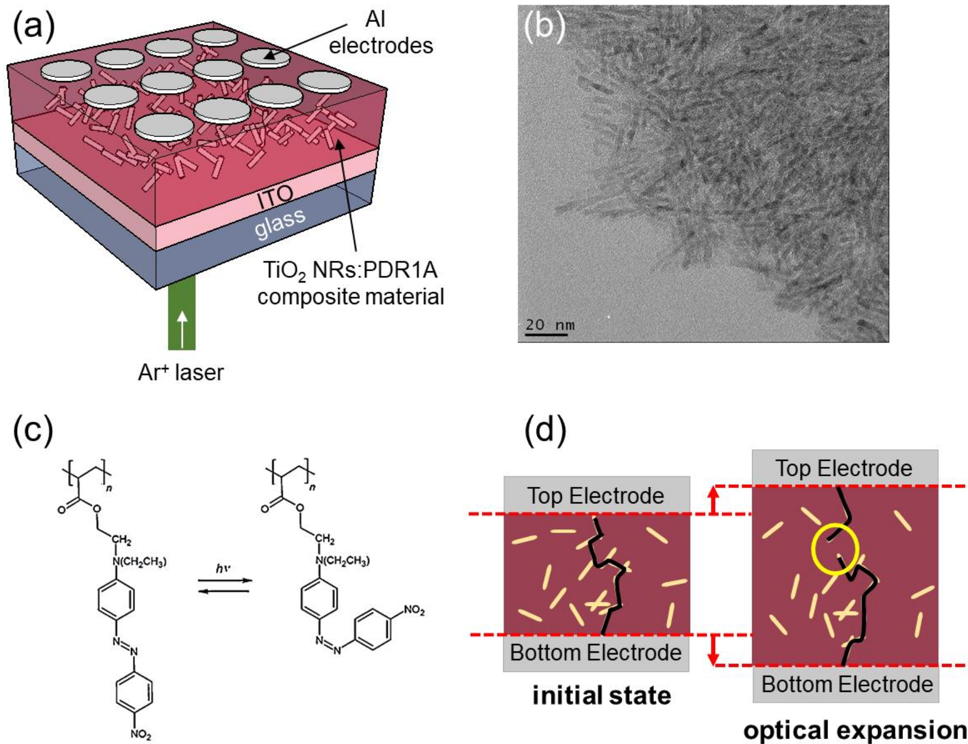

Fig. 1. (a) Schematic of the optical resistive memory device consisting of the nanocomposite PDR1A /TiO_2-NR film sandwiched between indium tin oxide (ITO) and aluminum (Al) electrodes. (b) TEM image of the TiO_2-NRs. (c) The *trans-cis* photochemical isomerization of the optically-active azopolymer (PDR1A). (d) The expansion of the polymer (PDR1A/TiO_2-NR) film due to the *trans-cis* photochemical isomerization of the optically-active azopolymer (PDR1A) on illumination with polarized light (514 nm) breaks the partially-connected conductive pathways (black line) within the PDR1A /TiO_2-NR layer, thereby causing controlled shifts in the conduction properties of the test memristor devices. The presence of a high-resistance "breakpoint" within the PDR1A /TiO_2-NR film, caused by optical illumination, is indicated by the yellow circle.

III. Experimental Results and Discussion

Fig. 2 shows the I-V sweeps of test memristor devices incorporating three different polymer (PDR1A/TiO_2-NR) films with different TiO_2-NR mass concentrations (Rm =0.01 wt %, 0.05 wt% and 0.1 wt%). No forming step was needed to initiate memristor switching in the devices and the I-V sweeps, carried out between -1 V and +1 V, show that switching in the test memristor devices occurs at low voltages. A current compliance limit (10 mA) was used to protect the test memristor devices from electrical breakdown. It can be seen that the devices exhibit a bipolar switching behavior with a threshold voltage, and the ON and OFF currents increase with increasing concentration of the TiO_2-NRs. This is expected since the concentration of the conductive component is increased relative to that of the

insulating component.[8] In their pristine state the devices are initially in the high-resistance state (HRS) and then switch to a low-resistance state (LRS) at SET threshold voltages of approximately 0.2 V. Interestingly, the set voltage decreases from 0.22 V to 0.18 V, when the NR concentration increases from 0.01 wt% to 0.1 wt%, which potentially indicates that there are more critical "connection" points in the devices with higher concentrations of TiO_2-NRs and that some of these devices are energetically easier to manipulate with the applied field. On the reverse sweep, the devices remain in the LRS and switch back to the HRS at -1 V.

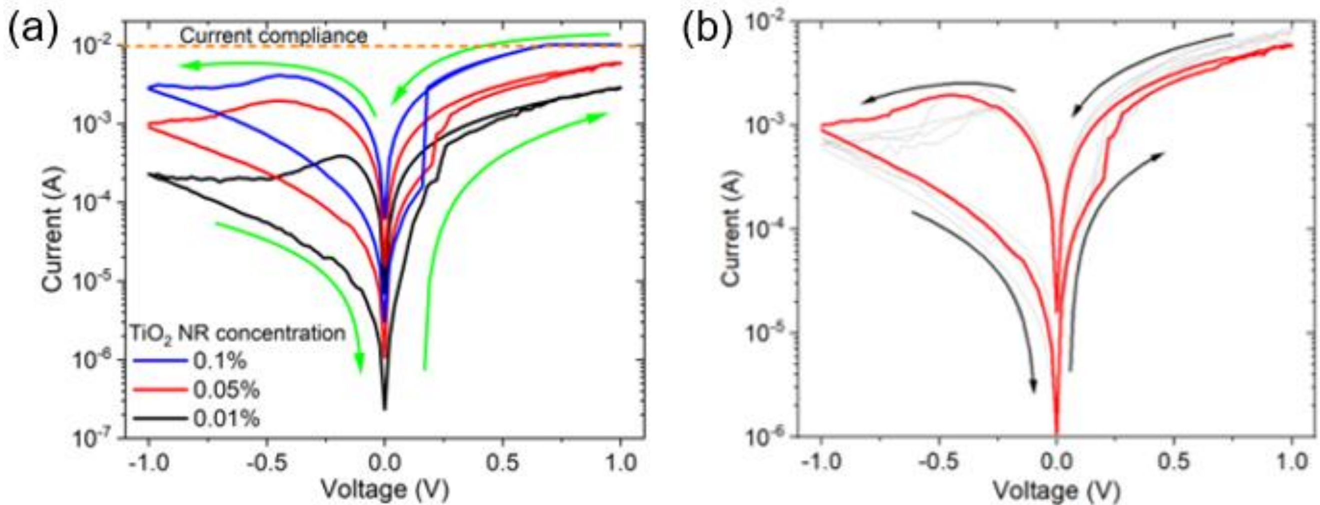

Fig. 2. (a) I-V sweeps for test memristor devices incorporating three polymer (PDR1A/TiO_2-NR) films with different mass concentrations of TiO_2-NRs (Rm = 0.01 wt %, 0.05 wt% and 0.1 wt%). The sweeps show that devices with a higher concentration of TiO_2-NRs are more conductive. (b) Repeated I-V cycles for a device with concentration Rm= 0.05 wt% and showing good repeatability between sweeps.

There are several distinct differences in the I-V curves and switching characteristics of the devices when compared to the two other published works in the literature that also utilize TiO_2 nanorods in memristor devices.[28,29] Both previous reports use a hydrothermal method to grow free-standing TiO_2 nanorod arrays on the bottom electrode of the devices. In this case, fluorine-doped tin oxide (FTO) is used as the growth substrate and bottom electrode as this results in perpendicular growth of TiO_2 nanorods. Although the hydrothermal method can produce nanorods with better stoichiometry and fewer crystalline defects, the *in-situ* growth of the nanorods within the device is more complex, slower and not well suited to upscaling for commercial applications. In comparison, the novel surface-stabilized nanorods used in this work can be easily dispersed in common solvents at relatively high concentration allowing the fabrication of devices by spin-coating, which is fast, simple and low-cost. Similar to our devices, forming steps were also not needed to initiate device switching in the previous reports. However, both articles report highly asymmetric I-V curves. This arises from the asymmetric device architecture, which consists

of nanorods grown on only one of the electrodes. Also, in contrast to our devices that switch at low potentials of ± 1 V, switching in this previous work required much larger potentials, up to $\pm$ 4 V. This is a consequence of the much thicker active switching material in these devices. This is set by the nanorod lengths, which ranged from 0.55 μm to 4.25 μm. Thicker active layers generally result in smaller electric fields and currents, which means high potentials need to be applied to switch between resistive states.

In the earliest of the two reports,[29] significantly large bipolar switching was found only for nanorods with lengths smaller than 3 μm. This was found to be related to the synthesis approach, whereby the oxygen defect concentration in the nanorods was found to decrease with increasing nanorod height. A space charge limited current mechanism associated with the oxygen vacancies was found to explain the I-V behavior of the devices. In the case of the more recent report,[28] time-dependent measurements showed the devices to have a highly volatile memory behavior, which in some cases gave retention times of only several seconds.

One of the main aims of this study was to impart optical switching in the memristor devices. Fig. 3a) shows the combined effect of both optical and electronic switching on the test devices. It demonstrates how optical irradiation can be used to modify the OFF/ON ratio of the memristors' resistance by almost three orders of magnitude. The plot shows the effect of optical irradiation on the I-V properties of a test memristor device with the lowest concentration (R_m of 0.01%.) of TiO_2-NRs. Irradiation by circularly polarized light, 30 minutes, photo-expands the PDR1A layer in the vertical direction causing the resistance OFF/ON ratio to improve by increasing/decreasing the ON/OFF currents. Subsequent irradiation by linearly polarized light for 15 minutes causes the composite PDR1A-TiO_2-NR layer to contract, which shifts the OFF/ON resistance ratio back towards the original (lower) value. A similar effect can also be observed in the control device, which consists of just PDR1A and without the TiO_2 nanorods. The change in current, before and after irradiation by circularly polarized light, can be attributed to just the change in the thickness of the irradiated PDR1A-TiO_2-NR film, Fig. 3b). The control device, incorporating the PDR1A film without TiO_2-NRs, exhibits very low conductivity, as expected for an insulating material, and no resistive switching effects are observed.

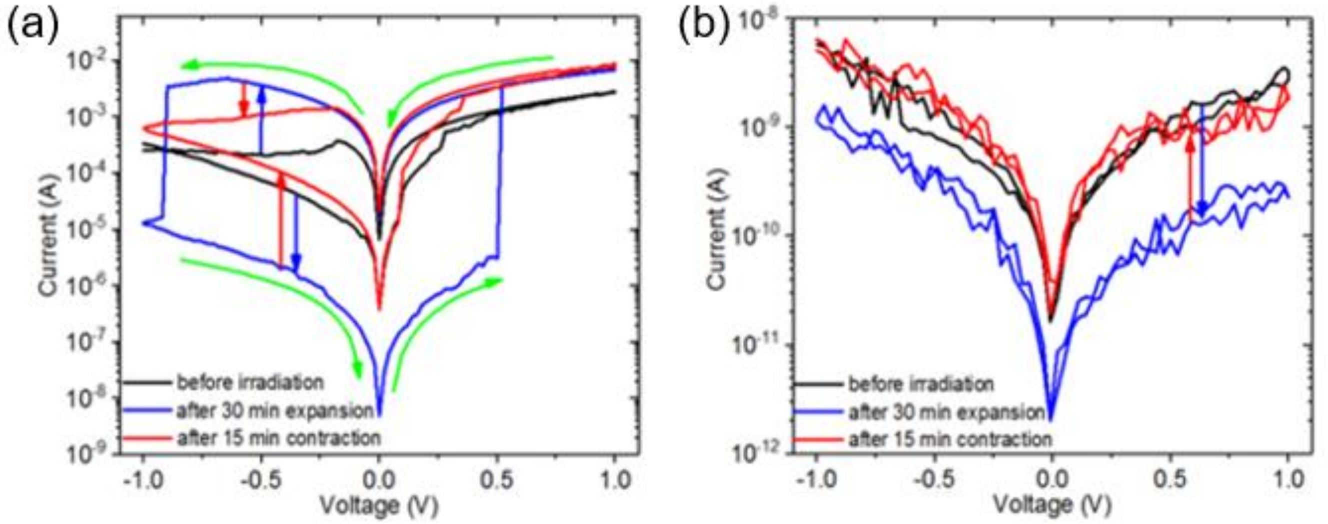

Fig. 3. (a) I-V sweeps for a test memristor device with the lowest concentration (R_m of 0.01%.) of TiO_2-NRs before irradiation (black curve), after expansion (blue curve) and after contraction (red curve). (b) I-V sweeps for a control device, incorporating the PDR1A film without TiO_2-NRs, which shows a very small conductance (small current) and only a minor change in this property after illumination and expansion of the PDR1A polymer film.

IV. Modelling

A. General Framework

In order to further analyse the results obtained for these test memristor devices, we have studied an approach proposed by Picos et al. in the literature.[41,42] In this case, the basic model of the memristive device has been derived using a framework[43] in which memristors are described by charge and flux instead of current and voltage.[44–52] The charge Q is defined as the first momentum of the current and the flux ϕ is defined accordingly for the voltage as follows[43]

$$Q(t) = \int_{-\infty}^{t} I(\tau) d\tau \tag{1}$$

and

$$\phi(t) = \int_{-\infty}^{t} V(\tau) d\tau \tag{2}$$

Since the device under study is assumed a memristor,[53] we have applied a simple piecewise model[54,55] to fit experimental measurements. The modelling of the set and reset phases of the I–V curve are represented by the time derivative of the charge given by

$$I(\phi, V) = V \cdot G(\phi) \tag{3}$$

Considering a full reset/set cycle in the memristive nanorod-polymer device as a result of applying a triangular voltage signal, negative in case of reset and positive in case of set, we have modelled the

conductance G of each transition, either reset or set, by taking two pairs of measured values in order to calculate the parameters needed.

The model parameters for any reset cycle depend on the reset and break points, while those for any set cycle depend on the set and complete points.[54,55] Fig. 4 shows experimental conductance vs. flux for a full reset/set cycle with the points we used to extract the model parameters. The reset point (rst) is determined as the point corresponding to maximum current I_{max} during the reset cycle. The break point (brk) is the inflection point for the charge, and can be found by taking the second derivative (d^2Q/dt^2), which is the first derivative of the current. The minimum value of this derivative corresponds to the break point. The decrease point (*d*) corresponds to the maximum applied voltage during the reset cycle. The maximum point (*max*) corresponds to the final values where the flux and charge have their maximum values during the reset cycle.[55].

The set point (set) represents the first inflection point of the current during the set transition which can be found by taking the second derivative (d^2I/dt^2), the complete point (com) represents the point where the current considerably increases when the device changes from high resistance state (HRS) to low resistance state (LRS).

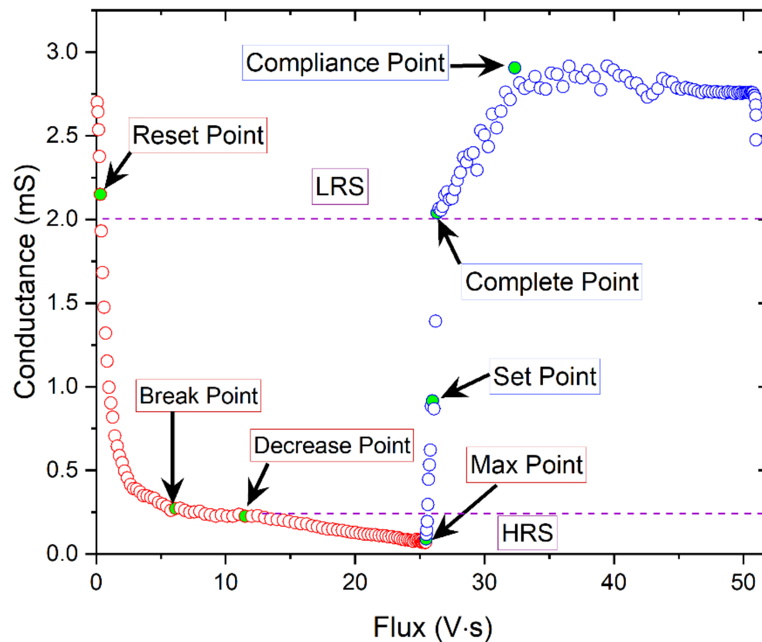

Fig. 4: Experimental conductance vs. flux for full reset / set cycle (data corresponds to the lower branch of the 0.01% TiO_2 data in Fig. 5).

The conductance before and after the reset transition has two almost constant levels. The first is high, which we attribute to a metallic-like conductance, $G_{rst,}$ in Fig.4, (see arrows and labels on the graph

denoting the Reset Point and low resistance state, LRS) and the second is low, which we attribute to hopping-like conductance[56], G_{brk}. The change between these two states is expected to be related to the changes in the barrier between the nanorods and the polymer. This idea is further supported by the fact that a physical change in the polymers through illumination also causes a change in the conductivities of these states. Up to the reset point the conductance is high, and at this point the high conductance G_{rst} starts to decrease during the process that breaks the conductive path and creates a gap up to the break point, where at this point the conductance becomes low G_{brk}. It can be noticed that the transition process from LRS to HRS during the reset cycle starts at the reset point, which corresponds to the LRS, and ends at the break point, which corresponds to the HRS. During this process, a dissolution of the conductance path occurs to form a high resistance gap.

Applying our model, the device conductance during a full reset cycle as a result of applying a negative triangular signal can be written as follows

$$G(\phi) = \begin{cases} n_1 \cdot \frac{Q_{rst}}{\phi_{rst}^{n_1}} \cdot \phi^{n_1 - 1} & (0 \le \phi \le \phi_{rst}) \\ n_2 \cdot \frac{Q_{rst}}{\phi} & (\phi_{rst} \le \phi \le \phi_{brk}) \\ \frac{Q_d - Q_{brk}}{\phi_d - \phi_{brk}} & (\phi_{brk} \le \phi \le \phi_d) \\ n_3 \cdot \frac{Q_{max}}{\phi_{max}^{n_3}} \cdot \phi^{n_3 - 1} & (\phi_d \le \phi \le \phi_{max}) \end{cases} \quad (4)$$

It should be noted that the conductivity is almost constant after passing the break point, as described in the third part of the last equation ($\phi_{brk} \le \phi \le \phi_d$), where it is almost equal to the conductivity at the break point. After passing the decrease point, the conduction mechanism changes again, leading to a non-constant conductance, that is modelled in the fourth part of the last equation.

From Fig.4, it is apparent the hopping conductance of the HRS at the beginning of the set transition (0.1 mS at around 25 V.s), when a negative voltage input signal would be applied, is smaller than the conductance at the end of the reset cycle. This means the conductance depends on the polarity of the applied signal (direction and magnitude of the applied electrical field).[57] Then, the hopping conductance starts to increase slowly by increasing the amplitude value of the negative applied voltage signal as a result of increasing the magnitude of the electrical field. This electrical field up to the set point is not sufficient to start the construction of a new conductive path. At the set point, the conductance G_{set} is still smaller than the conductance of the broken conductance path in the reset transition G_{brk}. However, filling the gap or reducing the hopping conductance and increasing the metallic-like conductance starts at the set point up to the complete point (2.9 mS at around 32 V·s). The set point is defining the beginning of the conductive path formation. where the complete point defining the conductance path formation.

After forming the new conductive path and passing the complete point, the current increases. It has to be pointed out that the process of the set transition may be limited by the instrumental compliance current Ic that controls the value of the applied voltage Vc in order to prevent a destructive breakdown of the new conductive path. This may lead to a different behaviour than expected, since the actual applied voltage is different from the expected one. This current controls the conductive path size and as a result the reset current in the next reset cycle, which determines the reset point.[58,59] The process of filling the gap (behaviour from set point to complete point) during the set transition in the device under study is faster than the process of breaking the conductive path (behaviour from reset point to break point) during the reset transition. At the end of the set transition, the conductance is a metallic-like and almost is equal to the high conductance during the reset transition $Grst$. Finally, the device conductance during a full set cycle as a result of applying a positive triangular signal can be written as following

$$G(\phi) = \begin{cases} n_4 \cdot \frac{Q_{set}}{\phi_{set}^{n_4}} \cdot \phi^{n_4 - 1} & (0 \geq \phi \geq \phi_{set}) \\ n_5 \cdot \frac{Q_{set}}{\phi_{set}} \cdot e^{n_5 \cdot \left(\frac{\phi}{\phi_{set}} - 1\right)} & (\phi_{set} \geq \phi \geq \phi_{com}) \\ \frac{I_c}{V_c} & (\phi_{com} \geq \phi \geq \phi_c) \\ n_1 \cdot \frac{Q_{rst}}{\phi_{rst}^{n_1}} \cdot \phi^{n_1 - 1} & (\phi_c \geq \phi \geq \phi_{max}) \end{cases} \quad (5)$$

This correlation between the internal model parameters correspond to the points in Fig. 4 has already been discussed in the literature[60,61] and has been used to implement Monte Carlo models.[62,63]

B. Effect of the TiO2-NR concentration

We applied the model based on equations (3-5) to fit the results of experimental measurements of three reset/set cycles for devices with different concentrations. Fig. 5 shows modelled current *vs.* voltage and Table I provides the extracted parameters values that have been used in the implementation of the model, further details on the parameter's extraction procedure can be found elsewhere.[55] The I-V characteristics in Fig. 5 are derived from the conductance modelling, and show how the change in the threshold switching voltage is also well reproduced.

Parameter	Extracted value
n_1	0.95
n_2	1.05
n_3	0.5
n_4	0.9
n_5	1.02

Table I: The parameters and their corresponding values that have been used in the implementation of the model.

Concentration %	ϕ_{rst} (V.s)	Q_{rst} (C)	ϕ_{brk} (V.s)	Q_{brk} (C)	ϕ_d (V.s)	Q_d (C)	ϕ_{max} (V.s)	Q_{max} (C)	ϕ_{set} (V.s)	Q_{set} (C)
0.1	2.42	0.027	8.82	0.06	12	0.069	25.5	0.097	0.32	2.81e-4
0.05	2.42	0.013	14.455	0.034	12	0.032	25.5	0.041	0.5	6.71e-4
0.01	0.41	0.001	3.38	0.003	12	0.006	25.5	0.008	0.72	4.94e-4

Table II: The model parameters at reset and set points values for different concentrations.

We observe that the conductance increases with increasing TiO_2-NR concentration. On the other hand, more power is needed for the dissolution of conductive paths when the TiO_2-NR concentration is higher. As a result, the points in Fig. 4 change with increasing TiO_2-NR concentration, for instance, the reset point corresponding to the maximum current during the reset cycle and increasing TiO_2-NR concentration will increase the magnitude of this maximum current. The fast transition between the HRS and the LRS, as shown in Fig. 4, is remarkable and caused by the extremely fast creation mechanism, which is limited by the compliance current. Also, it is observed that the conductance for reset/set cycle is a function of the flux, in other words, the magnitude and the polarity of the applied voltage and how long it has been applied (Fig. 4).

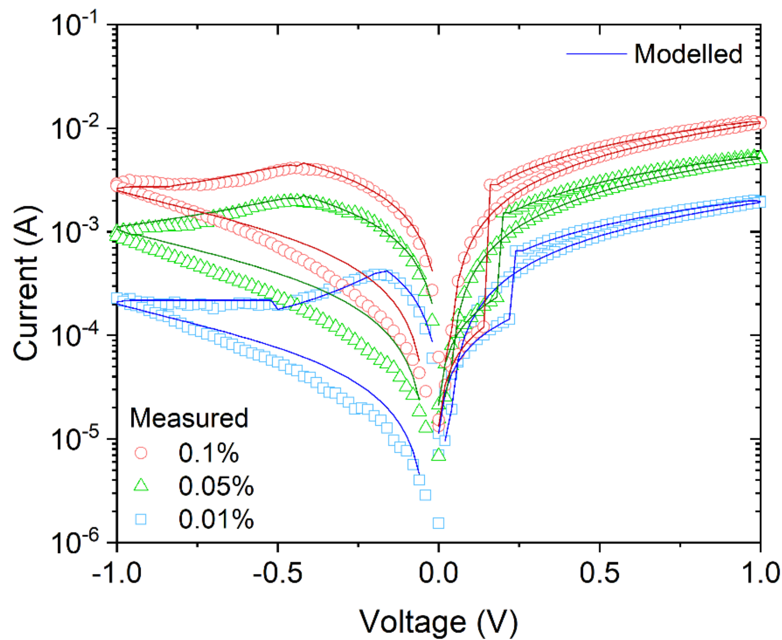

Fig. 5. Experimental data (symbols) and modelled (line) current vs. voltage for devices with different concentrations of TiO_2 NRs in PDR1A (using logarithmic scale for current).

C. Light Impact Model

The effect of illumination has been modelled in a similar way to a previous approach,[64,65,66] by assuming that the effects caused by the illumination are decoupled from the electrical behaviour Here, we have assumed that this effect can be modelled as a multiplicative factor in the conductance by

$$G(\phi, P_L^+, P_L^-, t) = \xi(P_L^+, P_L^-, t) \cdot G(\phi) \tag{6}$$

where $\xi(P_L^+, P_L^-, t)$ is the multiplicative factor described by a differential equation as follows

$$\frac{d\xi(P_L^+, P_L^-, t)}{dt} = a_1 \cdot P_L^+ - a_2 \cdot P_L^- \tag{7}$$

where a_1, a_2 represent the light energy absorption coefficient for the expansion and contraction of the polymer, respectively. This assumption is equivalent to assume a change in conductance which is linearly proportional to the absorbed energy.

In the above equation, P_L^+ is the power corresponding to the expanding polarization light and P_L^- is the contracting light power. The initial value of ξ with no previous illumination is obviously ξ=1. Experimentally, we have found that after a first illumination period (expanding), ξ = 3.12, and after the contracting period ξ = 2.49. With this assumption, and with the illumination data provided in the experimental section, we obtained a_1=0.001733 s^{-1}, and a_2=0.00070 s^{-1} which indicates a much faster effect of the expansion mechanism than that of contraction. The power dissipated by the device during a voltage sweep is

$$\begin{aligned} P(\phi, P_L^+, P_L^-, t) &= V(t)^2 \cdot G(\phi, P_L^+, P_L^-, t) \\ &= \xi(P_L^+, P_L^-, t) \cdot V(t)^2 \cdot G(\phi) \end{aligned} \tag{8}$$

where the input voltage signal was the same for all sweeps, and the total energy dissipated can be calculated according to

$$E(\phi, P_L^+, P_L^-, t) = \int_0^t P(\phi, P_L^+, P_L^-, \tau) d\,\tau \tag{9}$$

In our case, since the illumination was constant during the electrical measurement period (thus making ξ a constant), we can rewrite the last equation as following

$$E(\phi, P_L^+, P_L^-, t) = \xi(P_L^+, P_L^-, t) \cdot \int_0^{t1} V(t)^2 \cdot G(\phi) \cdot d\,\tau \tag{10}$$

where t_1 corresponds to the illumination intervals discussed in the experimental section. Notice that the term $V(t)^2 \cdot G(\phi)$ corresponds to the power in the case that the device has not been exposed to lighting.

To investigate the quality of the model, equation (6) was simulated and applied to the data in Fig 3a), which plots current-voltage sweeps before and after irradiation to light. Notice that the parameters of the model are kept constant, and assumed to be nearly independent of the illumination. The resulting data and simulation are shown in Fig. 6 and Fig. 7, for the case of power and energy, respectively. In both cases, very good fits of the model to the data was obtained. In addition, it is also worth pointing out that we have been able to decouple the variations caused by the illumination in the reset and set points seen the current-voltage. In the charge-flux model, these variations are simply absorbed as changes in the conductance. Since the effect of illumination has been decoupled from the electrical equations, this fitting seems to reinforce the idea that the conduction mechanism itself does not change with illumination but instead the illumination results in a modification of the conduction pathway, most likely a change in a critical resistive barrier between two nanorods, as shown in Fig. 1d.

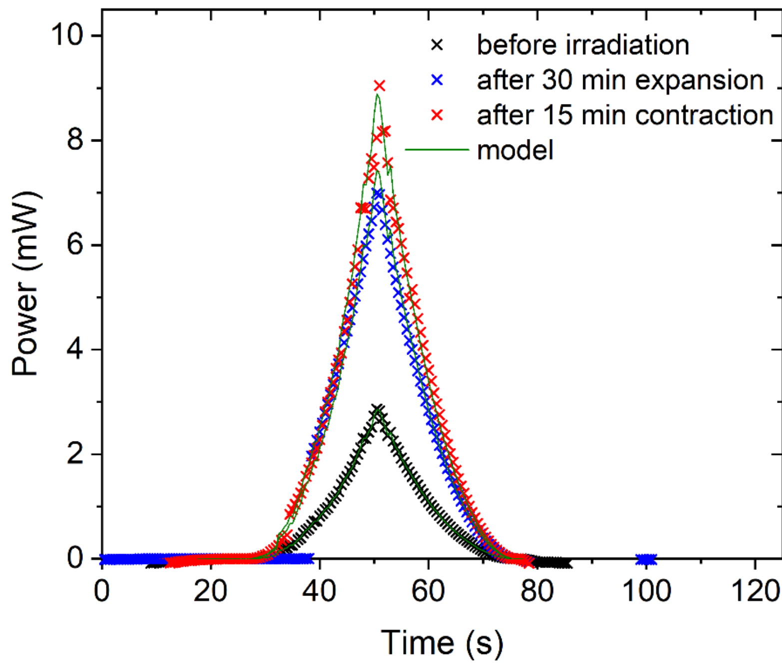

Fig. 6. Power calculated from experimental current-voltage measurements and modelled (green lines) vs. time for a device consisting of TiO_2 NRs at Rm = 0.01% embedded within PDR1A before irradiation (black), after expansion (blue) and after contraction (red).

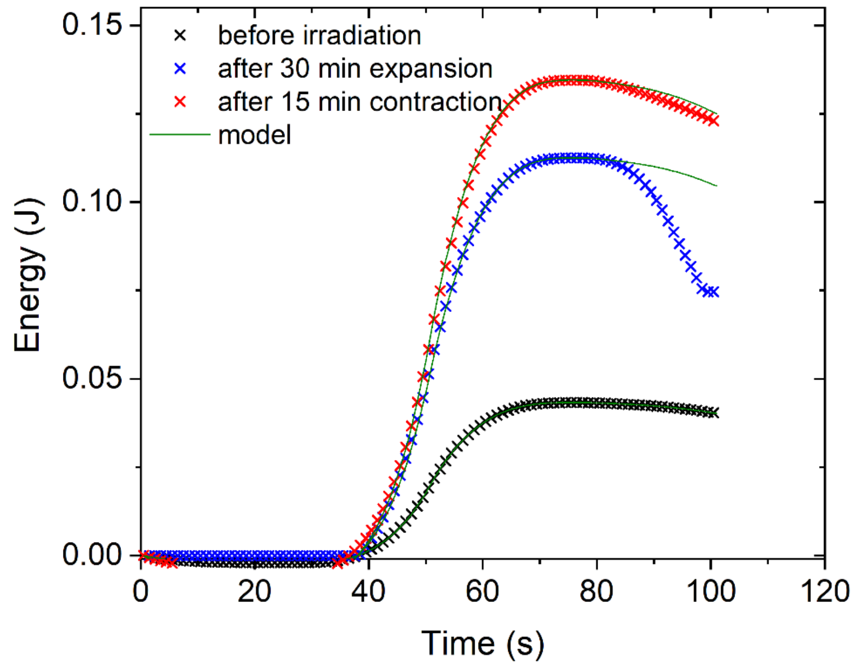

Fig. 7. Energy calculated from experimental current-voltage measurements and modelled (green lines) *vs*. time for a device with an active layer of semiconductor TiO_2-NRs at Rm = 0.01 wt% embedded within an insulating PDR1A polymer matrix, before irradiation (black), after expansion (blue) and after contraction (red).

IV. Conclusion

In summary, a unique nanocomposite resistive-switching material (PDR1A/TiO_2-NRs), consisting of an insulating, but photoactive, azopolymer matrix (PDR1A) and a very low concentration (~0.1 wt%) of surface-stabilized, titanium dioxide nanorods (TiO_2-NRs) as an inorganic semiconductor, has been developed and utilized within a device that shows both electrical and optical switching. This approach takes advantage of the rod-like shape and relatively-high aspect ratio of the TiO_2-NRs to achieve memristor switching with an extremely low mass-fraction (~0.1 wt%) of TiO_2-NRs within the PDR1A polymer matrix. The new photoactive device exhibits both electronic memristor switching and reversible, polarization-dependent optical switching due to the photoactive nature of the azobenzene moieties in PDR1A, which become preferentially aligned or misaligned depending on the polarization of incident light. Absorption of this irradiation causes an expansion of the PDR1A/TiO_2-NRs film that modulates,

and in some cases completely interrupts, the conduction pathway through the device. The morphology and concentration of the TiO_2-NRs within the PDR1A polymer matrix have been chosen so that just a few conduction pathways exist within the photoactive PDR1A/TiO_2-NRs nanocomposite layer, which provides very sensitive control of the electronic conduction and memristor switching of the device by illumination of monochromatic light of the correct wavelength and intensity. This effect is also shown to be reversible by changing the polarization state of the incident light. A charge-flux memristor model incorporating piecewise fits, to take into consideration the highly non-linear aspects of the switching behavior in the PDR1A/TiO_2-NRs active layer successfully reproduces the current-voltage hysteresis loops and threshold switching properties of the device. A further modification to take into consideration the expansion and contraction of the photoactive azopolymer, due to absorption of monochromatic laser light, is included in an optimized model that successfully reproduces the observed changes in the conduction properties of the test devices, both before and after optical illumination.

Acknowledgements

We would like to sincerely thank the Iraqi Ministry of Higher Education and Scientific Research (University of Baghdad) for supporting and part funding of this work.

References

(1) Zhai, Y.; Yang, X.; Wang, F.; Li, Z.; Ding, G.; Qiu, Z.; Wang, Y.; Zhou, Y.; Han, S. T. Infrared-Sensitive Memory Based on Direct-Grown MoS2 –Upconversion-Nanoparticle Heterostructure. *Adv. Mater.* **2018**, *30*, 1803563. https://doi.org/10.1002/adma.201803563.

(2) Mao, J.; Zhou, L.; Zhu, X.; Zhou, Y.; Han, S. Photonic Memristor for Future Computing : A Perspective. *Adv. Opt. Mater.* **2019**, *1900766*, 1–15. https://doi.org/10.1002/adom.201900766.

(3) Nicolosi, L.; Blug, A.; Abt, F.; Tetzlaff, R.; Höfler, H.; Carl, D. Real-Time Control of Laser Beam Welding Processes: Reality. In *Focal-Plane Sensor-Processor Chips*; Zarándy, Á., Ed.; Springer-Verlag: New York, 2011; pp 261–281. https://doi.org/10.1007/978-1-4419-6475-5.

(4) Müller, J.; Wittig, R.; Müller, J.; Tetzlaff, R. An Improved Cellular Nonlinear Network Architecture for Binary and Grayscale Image Processing. *IEEE Trans. Circuits Syst. II - Express Briefs* **2018**, *65* (8), 1084–1088. https://doi.org/10.1109/TCSII.2016.2621773.

(5) Chua, L. O. Memristor, Hodgkin-Huxley, and Edge of Chaos. *Nanotechnology* **2013**, *24* (38), 383001. https://doi.org/10.1088/0957-4484/24/38/383001.

(6) Šuch, O.; Klimo, M.; Kemp, N. T.; Škvarek, O. Passive Memristor Synaptic Circuits with Multiple

Timing Dependent Plasticity Mechanisms. *AEU - Int. J. Electron. Commun.* **2018**, *96*, 252–259. https://doi.org/10.1016/j.aeue.2018.09.025.

(7) He, H. K.; Yang, R.; Zhou, W.; Huang, H. M.; Xiong, J.; Gan, L.; Zhai, T. Y.; Guo, X. Photonic Potentiation and Electric Habituation in Ultrathin Memristive Synapses Based on Monolayer MoS 2. *Small* **2018**, *14*, 1800079. https://doi.org/10.1002/smll.201800079.

(8) Jaafar, A. H.; O'Neill, M.; Kelly, S. M.; Verrelli, E.; Kemp, N. T. Percolation Threshold Enables Optical Resistive-Memory Switching and Light-Tuneable Synaptic Learning in Segregated Nanocomposites. *Adv. Electron. Mater.* **2019**, *5* (7), 1900197. https://doi.org/10.1002/aelm.201900197.

(9) Jaafar, A. H.; Gray, R. J.; Verrelli, E.; O'Neill, M.; Kelly, S. M.; Kemp, N. T. Reversible Optical Switching Memristors with Tunable STDP Synaptic Plasticity: A Route to Hierarchical Control in Artificial Intelligent Systems. *Nanoscale* **2017**, *9* (43), 17091–17098. https://doi.org/10.1039/c7nr06138b.

(10) Jaafar, A. H.; Kemp, N. T. Wavelength Dependent Light Tunable Resistive Switching Graphene Oxide Nonvolatile Memory Devices. *Carbon N. Y.* **2019**, *153*, 81–88. https://doi.org/10.1016/j.carbon.2019.07.007.

(11) Verrelli, E.; Gray, R. J.; O'Neill, M.; Kelly, S. M.; Kemp, N. T. Microwave Oven Fabricated Hybrid Memristor Devices for Non-Volatile Memory Storage. *Mater. Res. Express* **2014**, *1* (4), 046305. https://doi.org/10.1088/2053-1591/1/4/046305.

(12) Gray, R. J.; Jaafar, A. H.; Verrelli, E.; Kemp, N. T. Method to Reduce the Formation of Crystallites in ZnO Nanorod Thin-Films Grown via Ultra-Fast Microwave Heating. *Thin Solid Films* **2018**, *662* (30 September), 116–122. https://doi.org/10.1016/j.tsf.2018.07.034.

(13) Lee, C. T.; Yu, L. Z.; Chen, H. C. Memory Bistable Mechanisms of Organic Memory Devices. *Appl. Phys. Lett.* **2010**, *97* (4), 4–7. https://doi.org/10.1063/1.3467050.

(14) Jung, S. M.; Kim, H. J.; Kim, B. J.; Lee, H. H.; Kim, Y. S.; Yoon, T. S. Electrical Charging of Au Nanoparticles Embedded by Streptavidin-Biotin Biomolecular Binding in Organic Memory Device. *IEEE Trans. Inf. Theory* **1993**, *39* (3), 1071–1076. https://doi.org/10.1109/18.256519.

(15) Zhao, J. H.; Thomson, D. J.; Pillai, R. G.; Freund, M. S. Dynamic Resistive Crossbar Memory Based on Conjugated Polymer Composite. *Appl. Phys. Lett.* **2009**, *94* (9). https://doi.org/10.1063/1.3080617.

(16) Jaafar, A. H.; Gee, A.; Hamza, A. O.; Eling, C. J.; Bouillard, J.-S. G.; Adawi, A. M.; Kemp, N. T. Evidence of Nanoparticle Migration in Polymeric Hybrid Memristor Devices. In *2020 European Conference on Circuit Theory and Design (ECCTD)*; IEEE, 2020; pp 1–4. https://doi.org/10.1109/ECCTD49232.2020.9218360.

(17) Kemp, N. T.; Newbury, R.; Cochrane, J. W.; Dujardin, E. Electronic Transport in Conducting Polymer Nanowire Array Devices. *Nanotechnology* **2011**, *22* (10), 105202. https://doi.org/10.1088/0957-4484/22/10/105202.

(18) Lee, J.-K.; Cho, J. M.; Shin, W. S.; Moon, S. J.; Kemp, N. T.; Zhang, H.; Lamb, R. The Stability of PEDOT:PSS Films Monitored by Electron Spin Resonance. *J. Korean Phys. Soc.* **2008**, *52* (3), 621–626. https://doi.org/10.3938/jkps.52.621.

(19) Jabarullah, N. H.; Verrelli, E.; Mauldin, C.; Navarro, L. A.; Golden, J. H.; Madianos, L. M.; Kemp, N. T. Superhydrophobic SAM Modified Electrodes for Enhanced Current Limiting Properties in Intrinsic Conducting Polymer Surge Protection Devices. *Langmuir* **2015**, *31* (22), 6253–6264. https://doi.org/10.1021/acs.langmuir.5b00686.

(20) Tseng, R. J.; Huang, J.; Ouyang, J.; Kaner, R. B. Polyaniline Nanofiber / Gold Nanoparticle Nonvolatile Memory. *Nano* **2005**, *5* (May), 1–4. https://doi.org/10.1021/nl050587l.

(21) Anoop, G.; Panwar, V.; Kim, T. Y.; Jo, J. Y. Resistive Switching in ZnO Nanorods/Graphene Oxide Hybrid Multilayer Structures. *Adv. Electron. Mater.* **2017**, *3* (5), 1–9. https://doi.org/10.1002/aelm.201600418.

(22) Son, D. I.; Park, D. H.; Kim, J. Bin; Choi, J. W.; Kim, T. W.; Angadi, B.; Yi, Y.; Choi, W. K. Bistable Organic Memory Device with Gold Nanoparticles Embedded in a Conducting Poly(N -Vinylcarbazole) Colloids Hybrid. *J. Phys. Chem. C* **2011**, *115* (5), 2341–2348. https://doi.org/10.1021/jp110030x.

(23) Yang, Y. C.; Pan, F.; Liu, Q.; Liu, M.; Zeng, F. Fully Room-Temperature-Fabricated Nonvolatile Resistive Memory for Ultrafast and High-Density Memory Application. *Nano Lett.* **2009**, *9* (4), 1636–1643.

(24) Goswami, S.; Matula, A. J.; Rath, S. P.; Hedström, S.; Saha, S.; Annamalai, M.; Sengupta, D.; Patra, A.; Ghosh, S.; Jani, H.; et al. Robust Resistive Memory Devices Using Solution-Processable Metal-Coordinated Azo Aromatics. *Nat. Mater.* **2017**, *16* (12), 1216–1224. https://doi.org/10.1038/nmat5009.

(25) Dong, Y.; Yu, G.; McAlpine, M. C.; Lu, W.; Lieber, C. M. Si/a-Si Core/Shell Nanowires as Nonvolatile Crossbar Switches. *Nano Lett.* **2008**, *8* (2), 386–391. https://doi.org/10.1021/nl073224p.

(26) Strukov, D. B.; Snider, G. S.; Stewart, D. R.; Williams, R. S. The Missing Memristor Found. *Nature* **2008**, *453* (7191), 80–83. https://doi.org/10.1038/nature06932.

(27) Chua, L. Memristor-The Missing Circuit Element. *IEEE Trans. CIRCUIT THEORY* **1971**, *18* (5), 507–519.

(28) Ebenhoch, C.; Kalb, J.; Lim, J.; Seewald, T.; Scheu, C.; Schmidt-Mende, L. Hydrothermally Grown TiO2 Nanorod Array Memristors with Volatile States. *ACS Appl. Mater. Interfaces* **2020**, *12* (20), 23363–23369. https://doi.org/10.1021/acsami.0c05164.

(29) Yu, Y.; Wang, C.; Jiang, C.; Abrahams, I.; Du, Z.; Zhang, Q.; Sun, J.; Huang, X. Resistive Switching Behavior in Memristors with TiO2 Nanorod Arrays of Different Dimensions. *Appl. Surf. Sci.* **2019**, *485* (April), 222–229. https://doi.org/10.1016/j.apsusc.2019.04.119.

(30) Jaafar, A. H.; Gee, A.; Kemp, N. T. Nanorods Versus Nanoparticles: A Comparison Study of Au/ZnO-PMMA/Au Non-Volatile Memory Devices Showing the Importance of Nanostructure Geometry on Conduction Mechanisms and Switching Properties. *IEEE Trans. Nanotechnol.* **2020**, *19*, 236–246. https://doi.org/10.1109/TNANO.2019.2949759.

(31) Rau, H. *In Photochemistry and Photophysics*; J. K. Rabek, Ed.; CRC Press: Boca Raton, FL, 1990.

(32) Natansohn, A.; Rochon, P. Photoinduced Motions in Azo-Containing Polymers. *Chem. Rev.* **2002**, *102* (11), 4139–4175. https://doi.org/10.1021/cr970155y.

(33) Tanchak, O. M.; Barrett, C. J. Light-Induced Reversible Volume Changes in Thin Films of Azo Polymers: The Photomechanical Effect. *Macromolecules* **2005**, *38* (25), 10566–10570. https://doi.org/10.1021/ma051564w.

(34) Kumar, J.; Li, L.; Jiang, X. L.; Kim, D. Y.; Lee, T. S.; Tripathy, S. Gradient Force: The Mechanism for Surface Relief Grating Formation in Azobenzene Functionalized Polymers. *Appl. Phys. Lett.* **1998**, *72* (17), 2096–2098. https://doi.org/10.1063/1.121287.

(35) Karageorgiev, P.; Neher, D.; Schulz, B.; Stiller, B.; Pietsch, U.; Giersig, M.; Brehmer, L. From Anisotropic Photo-Fluidity towards Nanomanipulation in the Optical near-Field. *Nat. Mater.* **2005**, *4* (9),

699–703. https://doi.org/10.1038/nmat1459.

(36) Lee, S.; Kang, H. S.; Park, J. K. Directional Photofluidization Lithography: Micro/Nanostructural Evolution by Photofluidic Motions of Azobenzene Materials. *Adv. Mater.* **2012**, *24* (16), 2069–2103. https://doi.org/10.1002/adma.201104826.

(37) Saphiannikova, M.; Toshchevikov, V. Optical Deformations of Azobenzene Polymers: Orientation Approach vs. Photofluidization Concept. *J. Soc. Inf. Disp.* **2015**, *23* (4), 146–153. https://doi.org/10.1002/jsid.294.

(38) Alharthi, F. A.; Cheng, F.; Verrelli, E.; Kemp, N. T.; Lee, A. F.; Isaacs, M. A.; O'Neill, M.; Kelly, S. M. Solution-Processable, Niobium-Doped Titanium Oxide Nanorods for Application in Low-Voltage, Large-Area Electronic Devices. *J. Mater. Chem. C* **2018**, *6* (5), 1038–1047. https://doi.org/10.1039/C7TC04197G.

(39) Cheng, F.; Verrelli, E.; Alharthi, F. A.; Kelly, S. M.; O'Neill, M.; Kemp, N. T.; Kitney, S. P.; Lai, K. T.; Mehl, G. H.; Anthopoulos, T. Lyotropic "hairy" TiO2 Nanorods. *Nanoscale Adv.* **2019**, *1* (1), 254–264. https://doi.org/10.1039/c8na00054a.

(40) Cheng, F.; Verrelli, E.; Alharthi, F. A.; Das, S.; Anthopoulos, T. D.; Lai, K. T.; Kemp, N. T.; O'Neill, M.; Kelly, S. M. Solution-Processable and Photopolymerisable TiO2 Nanorods as Dielectric Layers for Thin Film Transistors. *RSC Adv.* **2020**, *10* (43), 25540–25546. https://doi.org/10.1039/d0ra04445h.

(41) Picos, R.; Roldan, J. B.; Al Chawa, M. M.; Garcia-Fernandez, P.; Jimenez-Molinos, F.; Garcia-Moreno, E. Semiempirical Modeling of Reset Transitions in Unipolar Resistive-Switching Based Memristors. *Radioengineering* **2015**, *24* (2), 421.

(42) Al Chawa, M. M.; Picos, R.; Roldan, J. B.; Jimenez-Molinos, F.; Villena, M. A.; de Benito, C. Exploring Resistive Switching-Based Memristors in the Charge–Flux Domain: A Modeling Approach. *Int. J. Circuit Theory Appl.* **2018**, *46* (1), 29–38. https://doi.org/10.1002/cta.2397.

(43) Corinto, F.; Civalleri, P. P.; Chua, L. O. A Theoretical Approach to Memristor Devices. *IEEE J. Emerg. Sel. Top. Circuits Syst.* **2015**, *5* (2), 123–132.

(44) Maldonado, D.; Gonzalez, M. B.; Campabadal, F.; Jimenez-Molinos, F.; Al-Chawa, M. M.; Stavrinides, S. G.; Roldan, J. B.; Tetzlaff, R.; Picos, R.; Chua, L. O. Experimental Evaluation of the Dynamic Route Map in the Reset Transition of Memristive ReRAMs. *Chaos, Solitons & Fractals* **2020**, *139*, 110288. https://doi.org/https://doi.org/10.1016/j.chaos.2020.110288.

(45) Al Chawa, M. M.; Picos, R.; Garcia-Moreno, E.; Stavrinides, S. G.; Roldan, J. B.; Jimenez-Molinos, F. An Analytical Energy Model for the Reset Transition in Unipolar Resistive-Switching Rams. In *Electrotechnical Conference (MELECON), 2016 18th Mediterranean*; 2016; pp 1–4.

(46) Al Chawa, M. M.; Stavrinides, S. G.; de Benito, C.; Bargallo, M.; Picos, R. A Non-Quasi Static Model for Reset Voltage Variation in Memristive Devices. In *2019 26th IEEE International Conference on Electronics, Circuits and Systems (ICECS)*; 2019; pp 1–4.

(47) Picos, R.; Garcia-Moreno, E.; Al Chawa, M. M.; Chua, L. O. Using Memristor Formalism in Semiconductor Device Modeling. In *Meeting Abstracts*; 2017; p 2048.

(48) Picos, R.; Al Chawa, M. M.; Roca, M.; Garcia-Moreno, E. A Charge-Dependent Mobility Memristor Model. In *Proceedings of the 10th Spanish Conference on Electron Devices, CDE'2015*; 2015.

(49) Al Chawa, M. M.; de Benito, C.; Roca, M.; Picos, R.; Stavrinides, S. G. Design and Implementation of Passive Memristor Emulators Using a Charge-Flux Approach. In *Circuits and Systems (ISCAS), 2018 IEEE International Symposium on*; 2018; pp 1–5.

(50) de Benito, C.; Al Chawa, M. M.; Picos, R.; Garcia-Moreno, E. A Procedure to Calculate a Dealy Model for Memristive Switches. In *Workshop on Memristor Technology, Design, Automation and Computing (MDAC) workshope at HiPEAC'2017*; 2017.

(51) Picos, R.; Roldan, J. B.; Al Chawa, M. M.; Jimenez-Molinos, F.; Villena, M. A.; Garcia-Moreno, E. Exploring {ReRAM}-Based Memristors in the Charge-Flux Domain, a Modeling Approach. In *Memristive Systems (MEMRISYS) 2015 International Conference on*; 2015; pp 1–2.

(52) Al Chawa, M. M.; Picos, R.; Tetzlaff, R. A Simple Memristor Model for Neuromorphic ReRAM Devices. In *2020 IEEE International Symposium on Circuits and Systems (ISCAS)*; 2020; p 1.

(53) Chua, L. Resistance Switching Memories Are Memristors. *Appl. Phys. A* **2011**, *102* (4), 765–783.

(54) Al Chawa, M. M.; de Benito, C.; Picos, R. A Simple Piecewise Model of Reset/Set Transitions in Bipolar ReRAM Memristive Devices. *IEEE Trans. Circuits Syst. I Regul. Pap.* **2018**, *65* (10), 3469–3480. https://doi.org/10.1109/TCSI.2018.2830412.

(55) Al Chawa, M. M.; Picos, R. A Simple Quasi-Static Compact Model of Bipolar ReRAM Memristive Devices. *IEEE Trans. Circuits Syst. II Express Briefs* **2020**, *67* (2), 390–394.

(56) Huang, P.; Liu, X. Y.; Chen, B.; Li, H. T.; Wang, Y. J.; Deng, Y. X.; Wei, K. L.; Zeng, L.; Gao, B.; Du, G.; et al. A Physics-Based Compact Model of Metal-Oxide-Based RRAM DC and AC Operations. *IEEE Trans. Electron Devices* **2013**, *60* (12), 4090–4097.

(57) Chang, Y.-F.; Chen, P.-Y.; Chen, Y.-T.; Xue, F.; Wang, Y.; Zhou, F.; Fowler, B.; Lee, J. C. Study of Polarity Effect in SiOx-Based Resistive Switching Memory. *Appl. Phys. Lett.* **2012**, *101* (5), 52111.

(58) Ielmini, D. Modeling the Universal Set/Reset Characteristics of Bipolar RRAM by Field-and Temperature-Driven Filament Growth. *IEEE Trans. Electron Devices* **2011**, *58* (12), 4309–4317.

(59) Zhou, F.; Chang, Y.-F.; Fowler, B.; Byun, K.; Lee, J. C. Stabilization of Multiple Resistance Levels by Current-Sweep in SiOx-Based Resistive Switching Memory. *Appl. Phys. Lett.* **2015**, *106* (6), 63508.

(60) Al Chawa, M. M.; Rodriguez-Fernandez, A.; Bargallo, M.; Campabadal, F.; de Benito, C.; Stavrinides, S.; Garcia-Moreno, E.; Picos, R. Waveform and Frequency Effects on Reset Transition in Bipolar ReRAM in Flux-Charge Space. In *International Conference on Memristive Materials, Devices & Systems (MEMRISYS 2017)*; 2017.

(61) Al Chawa, M. M.; Picos, R.; Covi, E.; Brivio, S.; Garcia-Moreno, E.; Spiga, S. Flux-Charge Characterizing of Reset Transition in Bipolar Resistive-Switching Memristive Devices. In *11th Spanish Conference on Electron Devices, 2017*; 2017.

(62) Picos, R.; Roldan, J. B.; Al Chawa, M. M.; Jimenez-Molinos, F.; Garcia-Moreno, E. A Physically Based Circuit Model to Account for Variability in Memristors with Resistive Switching Operation. In *Design of Circuits and Integrated Systems (DCIS), 2016 Conference on*; 2016; pp 1–6.

(63) Al Chawa, M. M.; Tetzlaff, R.; Picos, R. A Simple Monte Carlo Model for the Cycle-to-Cycle Reset Transition Variation of ReRAM Memristive Devices. In *2020 9th International Conference on Modern Circuits and Systems Technologies (MOCAST)*; 2020; pp 1–4.

(64) Papadopoulos, N. P.; Hatzopoulos, A. A.; Papakostas, D. K.; Picos, R.; Dimitriadis, C. A.; Siskos, S. A Light-Impact Model for p-Type and n-Type Poly-Si TFTs. *J. Disp. Technol.* **2009**, *5* (7), 265–272.

(65) Romero, A.; Jiménez, C.; González, J.; López-Varo, P.; Deen, M. J.; Jiménez-Tejada, J. A. Compact Modeling of the Effects of Illumination on the Contact Region of Organic Phototransistors. *Org. Electron.* **2019**, *70*, 113–121.

(66) Bley, S.; Castro-Carranza, A.; Tansey, E.; Seemann, W.; Gutowski, J. Impact of a Polystyrene-Based Passivating Interlayer on Hybrid Polymer/ZnO Nanowire Heterojunctions. In *Journal of Physics. Conference Series (Online)*; 2017; Vol. 864.

TOC Graphic (8.25*4.45cm)